Influence of Electron Transport Layer (TiO$_2$) Thickness and Its Doping Density on the Performance of CH$_3$NH$_3$PbI$_3$-Based Planar Perovskite Solar Cells

R. JEYAKUMAR [1,3,5] ATANU BAG [2] REZA NEKOVEI,[3]
and R. RADHAKRISHNAN[4]

1.—Materials and Devices Division, CSIR-National Physical Laboratory, New Delhi 110 012, India. 2.—School of Advanced Materials Science and Engineering, Sungkyunkwan University, Suwon, Gyeonggi-do 16419, Republic of Korea. 3.—Department of Electrical Engineering and Computer Science, Texas A&M University-Kingsville, Kingsville, TX 78363, USA. 4.—IBM CIC, Monroe, LA 71203, USA. 5.—e-mail: ramanuj@nplindia.org

Simulation studies are vital to understanding solar cell performance and in optimal device design for high-efficiency solar cells. Cell performance is sensitive to many factors, including device architecture, energy band alignment at the interfaces, materials used for photogeneration, charge extraction, doping density and thickness of various layers. The role of electron transport layer (ETL) thickness and its doping density on device performance is explored in this work. As the ETL thickness is increased from 10 nm to 200 nm, both fill factor (FF) and efficiency remain high up to 40 nm, at 0.85 and 28.04%, respectively, and beyond 40 nm, they decrease gradually due to a sharp increase in series resistance, reaching zero at 200 nm. However, J_{sc} and V_{oc} remained unchanged up to an ETL thickness of about 150 nm and 160 nm, respectively. These results were confirmed by contour plots of the simulated V_{oc}, J_{sc}, FF and efficiency results. We observed that when ETL approached 200 nm, J_{sc} and V_{oc} decreased to zero and 0.88 V, respectively. This can be attributed to very high series resistance and recombination in the cell. Donor concentration variation in the ETL from 10^{17}/cm^3 to 10^{20}/cm^3 has much less impact on J_{sc}, and V_{oc} remains unchanged. However, fill factor and efficiency improved, which might be due to an increase in conductivity in the ETL. Our result shows that for an optimized device, with an AM 1.5 spectrum, a cell efficiency of 29.64% was achieved with V_{oc}, J_{sc} and fill factor of 1.241 V, 28.70 mA/cm^2 and 0.83, respectively.

Key words: CH$_3$NH$_3$PbI$_3$, ETL thickness, contour map, ETL doping density, light I–V

INTRODUCTION

Perovskite-based solar cells are third-generation solar cells and represent an alternative to first generation (silicon) and second-generation (thin film) solar cells, due to low material cost, low thermal budget, simple fabrication processing methods, high efficiency and suitability for fabrication on flexible substrates.

Methylammonium lead iodide (CH$_3$NH$_3$PbI$_3$), known as MAPbI$_3$, is a leading organic–inorganic perovskite material used as an absorber, since MAPbI$_3$ is an efficient light-absorbing material in the visible region. High diffusion length,[1] ambipolar transport properties (i.e. MAPbI$_3$ can transport electrons and holes to their respective electrodes)

and suitable band gap of about 1.5 eV make MAPbI$_3$ a leading candidate for use as an absorber in solar cells. Using MAPbI$_3$ as absorber, record efficiency of 24.2% has been reported.[2] For absorber band gap of 1.5 eV, the Shockley–Queisser limit for a single-junction solar cell is $\sim$ 31.64%.[3]

There are two main structures used for fabrication, viz. planar structure and mesoporous structure. In the latter structure, metal oxide nanostructures (referred to as scaffolds) such as TiO$_2$, ZnO, SnO$_2$, Al$_2$O$_3$ or ZrO$_2$ are embedded within the perovskite absorber layer to enhance electron transport from the absorber to the top electrode through the electron transport layer (ETL). A mesoporous structure is used in the development of a dye-sensitized cell structure, where a perovskite layer is assisted by an underlying nanostructure made of metal oxide nanoparticles to improve light absorption. A disadvantage of using a mesoporous structure is the complicated high-temperature (450°C) process required for mesoporous structure formation,[4] and cell efficiency depends on pore size.[5] On the other hand, for a planar type, the maximum processing temperature is around 200°C, and cell efficiency for a planar type is higher than that of a mesoporous type. This suggests that a mesoporous type is not a prerequisite for high-efficiency solar cells. Therefore, a planar structure consisting of flat layer stacks was used in our simulation.

A perovskite solar cell works as follows: Incident light generates free electron–hole pairs in the absorber layer. Due to a concentration gradient, diffusion occurs toward the interface from the bulk region of the absorber,[6] and the presence of an electric field at the absorber interface causes drift (i.e. movement of charges under the influence of an electric field) on both sides. Note that drift allows charge carriers to cross to the other side where they are majority carriers. Therefore, by diffusion and drift mechanisms, electrons and holes travel toward the ETL and hole transport layer (HTL), respectively, and are collected by their respective p-type and n-type electrodes.

In terms of an ideal energy band diagram (Fig. 1), charge collection can be explained easily. Holes travelling toward the ETL are reflected back since valance band discontinuity (ΔE_{V1}) at the absorber/ ETL interface acts as a barrier for holes to flow to the ETL. Similarly, a high conduction band discontinuity (ΔE_{C2}) at the HTL/absorber interface restricts electrons from reaching the HTL. These two layers (ETL and HTL) are known as blocking layers for minority carriers. Due to a downward slope and negligible conduction band barrier (ΔE_{C1}) at the absorber/ETL interface, electrons can easily reach the ETL and n-type electrode. Holes also easily reach the HTL since ΔE_{V2} at the HTL/ absorber interface is very small for an appropriate absorber band gap of about 1.4 eV. From the absorber layer, charge carriers within the diffusion length reach the ETL and HTL and are collected by n-type and p-type contact electrodes, respectively.

Planar structure simulation requires three main layers, viz. ETL, absorber (perovskite) layer and HTL, and contact electrodes to collect charge carriers. Each layer thickness is in the nanometer range. A slight change in thickness can influence device performance. For example, a high ETL thickness causes series resistance and absorption losses in the device. Since light enters the device through the ETL, high transparency with a suitable band gap and thickness is required. For an ETL, n-TiO$_2$ is used due to its acceptable optical and electrical properties such as wide band gap of 3.2 eV, high transparency and high electron mobility. For practical device fabrication, TiO$_2$ layers are prepared by thermal oxidation of sputtered Ti film,[7] atomic layer deposition,[8] spray pyrolysis deposition,[9] sol–gel method[10] and spin-coating.[11]

Device simulation provides guidance for experimental fabrication. A systematic study has been performed in our simulation by varying TiO$_2$ film thickness and its doping density to find out its influence on device performance. The aim of this work is to design high-efficiency solar cells by fine-tuning the electrical properties by varying the ETL thickness and its doping density.

Device Structure and Simulation Details

Analysis of microelectronic and photonic structures (APMS), developed by Fonash et al.,[12] is generally used for simulation. In this work, perovskite solar cell simulation was carried out by using wxAMPS software,[13] which is an improved version of AMPS and solves the 1D problem. A device having the structure glass/fluorine-doped tin-oxide (FTO)/TiO$_2$/MAPbI$_3$/spiro-OMeTAD/Au was used for simulation. FTO and Au act as top and bottom contacts, respectively.

To determine the device performance, a set of basic equations, viz. Poisson's equation, and current continuity equations in steady state for electrons and holes are utilized in the wxAMPS program. These equations are given below:[14]

$$(1/q)(\delta/\delta x)[\varepsilon_x \delta \phi_x / \delta x] = \rho \qquad (1)$$

$$(1/q)(\delta J_e/\delta x) = -G(x) + R_n(x) \text{ for electrons} \qquad (2)$$

$$(1/q)(\delta J_h/\delta x) = G(x) - R_h(x) \text{ for holes} \qquad (3)$$

where x, ε, φ, q, ρ, J_n, J_p, G and R represent the position, dielectric constant of the material, local electric potential, electron charge, summed charge density (including free carriers, ionized impurities and trapped charges), electron current density, hole current density, optical (charge carrier) generation rate and total (charge carrier) recombination rate, respectively.
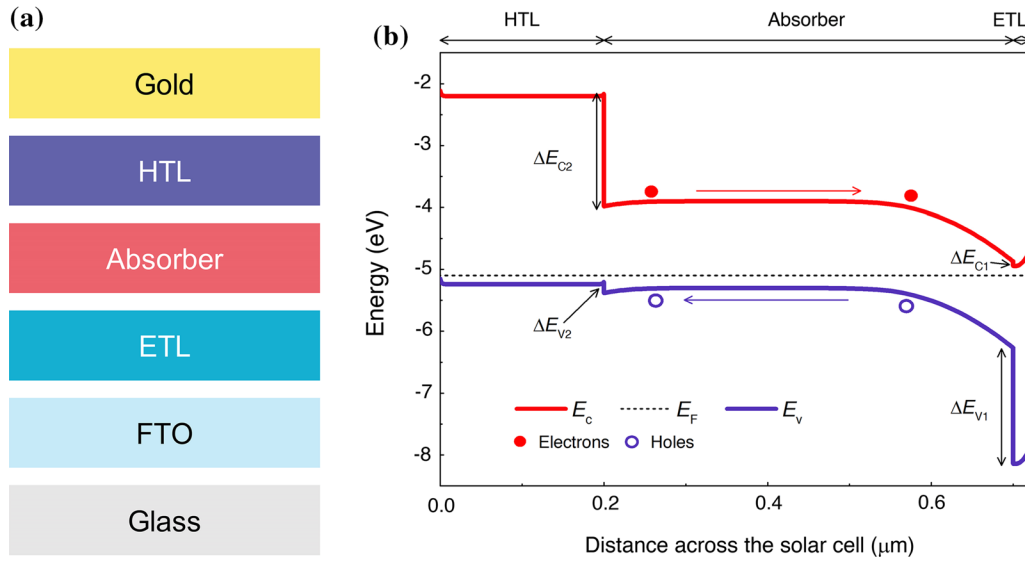
Fig. 1. (a) Schematic diagram of a perovskite solar cell, (b) an ideal energy band diagram of a planar perovskite solar cell [data from Ref. 19]. HTL, absorber and ETL correspond to p-spiro-OMeTAD, p-CH$_3$NH$_3$PbI$_3$ (band gap of 1.4 eV) and n-TiO$_2$. Negligible conduction band discontinuity (ΔE_{C1} 0.07 eV) at the ETL/absorber interface and valance band discontinuity (ΔE_{V2} 0.17 eV) at the HTL/absorber interface allow electrons and holes to easily reach the ETL and HTL, respectively. High valance band discontinuity (ΔE_{V1} 1.87 eV) at the ETL/absorber interface and conduction band discontinuity (ΔE_{C2} 1.81 eV) at the HTL/absorber interface block holes and electrons, respectively. For this reason, the ETL and HTL are known as hole-blocking layer and electron-blocking layer, respectively.

wxAMPS numerical simulation is performed[15] by simultaneously solving the above coupled nonlinear differential equations related to charge transport characteristics. Newton's and Gummel's methods are used to solve these equations.

Tunneling component models (trap-assisted tunneling and intra-band tunneling) are included in the wxAMPS program[13,16,17] for better simulation of heterojunction solar cells. In the trap-assisted tunneling model, carrier mobility is enhanced by an electric field present at the junction.[18] The intra-band tunneling model provides carrier transport across abrupt heterojunction interfaces. In the intra-band model,[17] thermionic emission as well as intra-band tunneling is considered. The wxAMPS simulation tool uses Newton's and Gummel's methods to improve stability by calculating intra-band tunneling.[13]

Since photogeneration and recombination mainly occur in the perovskite absorber layer, defects in the perovskite layer play an important role in determining the device performance. Various types of defect (donor-like, acceptor-like, etc.) parameters for the materials are defined in the simulation and reported elsewhere.[19] In the absorption layer, Gaussian-like distribution is more appropriate to describe the defect states.[20] Defects are located 0.6 eV above the top of the valance band with a density of 1×10^{17}/cm^3; characteristic energy of 0.1 eV is considered, and the electron and hole capture cross section is set to 1×10^{14}/cm^2.

The wxAMPS program determines the electron and hole concentration in the defect levels. The concentrations of trapped electrons and holes from all defects are incorporated into Poisson's equation, and the number of carriers involved in the recombination process are used in the continuity equations for free electrons and free holes.

In this work, the donor concentration in the ETL was varied from 1×10^{17}/cm^3 to 1×10^{20}/cm^3. Based on our previous work, the acceptor doping density in the absorber and HTL was fixed as 2.14×10^{17}/cm^3 and 10^{18}/cm^3, respectively.[21] The characteristic energy for tail states was 0.01 eV, and tail state density was 1×10^{14}/cm^3/eV. The thermal velocity for electrons and holes is set to 10^7 cm/s. The absorption coefficients for the ETL, absorber and HTL were obtained from Refs. 22–24.

Basic simulation parameters are shown in Table - I. Material parameters are chosen from experimental and theoretical results. Film thickness, carrier mobility and optical band gap for the materials are also given in Table I.

The simulated structure consists of three main layers, viz. electron transport layer, absorber layer and hole transport layer. Light I–V characteristics of the device were determined using an AM 1.5 solar spectrum, and light enters through the transparent conducting oxide (TCO). The reflection coefficients of the top and bottom surfaces were set to 0 and 1, respectively. ETL thickness and doping density were varied from 10 to 200 nm, and 10^{17}/cm^3 to 10^{20}/cm^3, respectively. The thickness and doping density of the absorber and HTL were fixed at 500 nm and 2.14×10^{17}/cm^3, and 200 nm and 10^{18}/cm^3, respectively.

Table I. Basic parameters used for perovskite solar cell simulation. TiO$_2$, MAPbI$_3$ and spiro-OMeTAD are used as ETL, absorber and HTL, respectively, as active layers in the simulation[25–38]

| Parameter	TiO$_2$	MAPbI$_3$	p-spiro-OMeTAD
Thickness (nm)	10–200	500	200
Band gap (eV)	3.26	1.4	3.0
Relative permittivity (ε_r)	9.0	32	3.0
Electron affinity (eV)	4.0	3.93	2.05
Defect density/cm^3	1×10^{15}	2.5×10^{13}	1×10^{15}
Effective density of states in the conduction band/cm^3	2.2×10^{18}	2.2×10^{18}	2.2×10^{18}
Effective density of states in the valence band/cm^3	1.8×10^{19}	1.8×10^{19}	1.8×10^{19}
Donor concentration/cm^3	$1 \times 10^{17-20}$	0	0
Acceptor concentration/cm^3	0	2.14×10^{17}	1×10^{18}
Electron mobility (cm^2/V s)	20	2	1×10^{-4}
Hole mobility (cm^2/V s)	10	2	2×10^{-4}
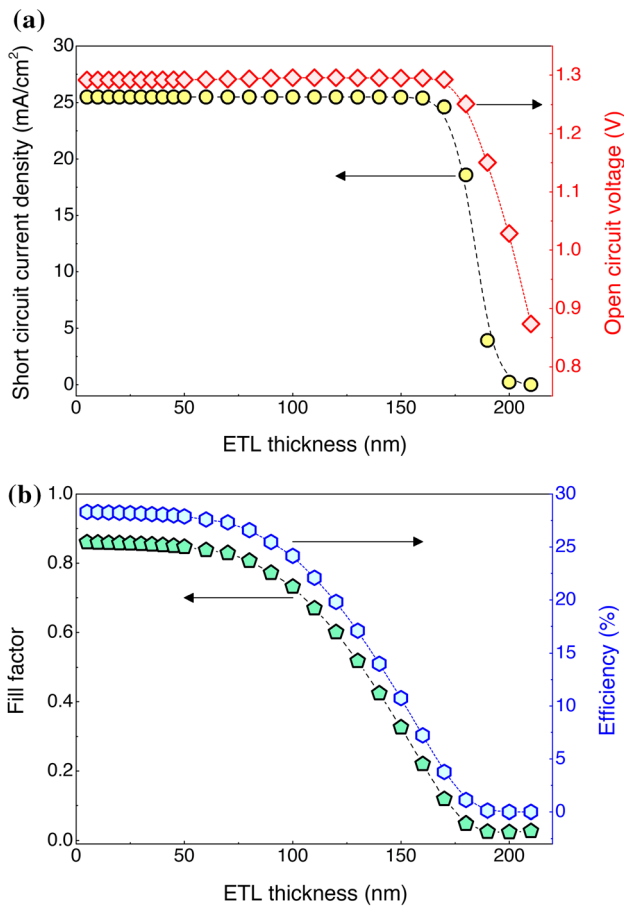
Fig. 2. Photovoltaic parameters as a function of ETL thickness: (a) J_{sc} and V_{oc}; (b) fill factor and efficiency. Fixed thickness of 500 nm and 200 nm was used for the absorber and HTL, respectively, in the simulation.

Results and Discussion

Wide-band-gap and highly transparent material is required for an ETL, and TiO$_2$ fulfills both requirements. It collects electrons from the absorber and block holes from reaching it. Figure 2 shows J_{sc}, V_{oc}, FF and efficiency as a function of TiO$_2$ layer thickness. Up to about 160-nm thickness, J_{sc} and V_{oc} remain constant at 25.4 mA/cm^2 and 1.29 V, respectively, and independent of ETL thickness, and then both decreases drastically as the TiO$_2$ thickness increases further (Fig. 2a). A sharp decrease in J_{sc} could be due to decrease in light transmittance through the TiO$_2$ layer and high series resistance in the cell. The decline in V_{oc} can be attributed to recombination due to poor charge carrier separation[39] at the interface between TiO$_2$ and the perovskite layer which might be due to high series resistance in the cell. J_{sc} and V_{oc} as a function of ETL thickness are in agreement with the contour plot shown later in this section.

A high ETL thickness (> 160 nm) can have effects in many ways: (1) restricts electron transport to FTO, (2) increases the recombination rate that reduces V_{oc}, and (3) adds series resistance to the device which affects the fill factor and cell efficiency. Figure 2b shows the fill factor and efficiency for ETL thickness between 10 nm and 200 nm. For TiO$_2$ thickness up to 40 nm, the fill factor and cell efficiency are almost constant at about 0.85 and 28.04%, respectively. As the thickness increases, electrons have to travel longer distance to reach the top electrode. Due to an extended path length, there is a high probability for electrons to recombine with minority carriers (holes). Therefore, cell efficiency decreases mainly due to a decrease in fill factor caused by an increase in series resistance. If the fill factor is low, series resistance is high and vice versa. Fill factor is a measure of series resistance. When the ETL thickness is ≥ 160 nm, fill factor become zero, and cell efficiency drops to zero. For high-performance solar cells, an ideal ETL thickness of about 40 nm is required for a high fill factor. As shown in Fig. 3, an increase in TiO$_2$ thickness causes an increase in series resistance in the cell from about 1 Ω cm^2 to about 10^6 Ω cm^2.

Figure 4 shows a contour map of the simulated J_{sc}, V_{oc}, FF and efficiency versus ETL thickness and absorber thickness. HTL thickness of 200 nm was used in device simulation. J_{sc} remains constant up to an ETL thickness of about 150 nm, corresponding

Influence of Electron Transport Layer (TiO$_2$) Thickness and Its Doping Density on the
Performance of CH$_3$NH$_3$PbI$_3$-Based Planar Perovskite Solar Cells

3537

to an absorber thickness of 500 nm (Fig. 4a). Beyond 150 nm, J_{sc} decreases to zero as the ETL thickness increases to 200 nm. This result is similar to Fig. 2a where J_{sc} is constant until ETL thickness is about 150 nm, after which it becomes zero as the thickness approaches 200 nm. Figure 4b shows a
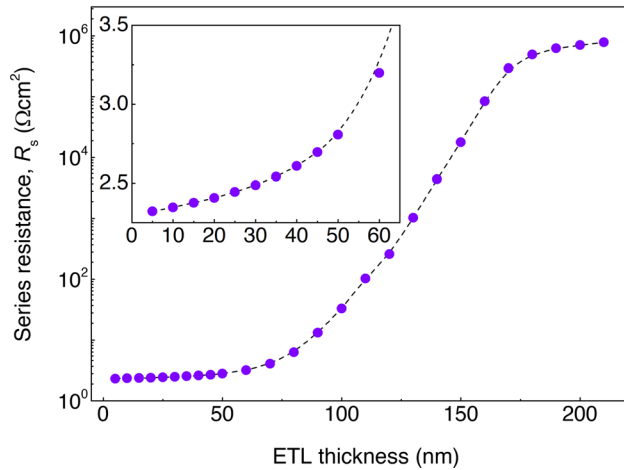

Fig. 3. Series resistance in the cell increases as ETL thickness increases. The inset shows series resistance of about 2.5 Ω cm^2 for an ideal thickness of 40 nm in the cell.

steady V_{oc} up to an ETL thickness of about 160 nm, and beyond that, V_{oc} decreases to $\sim$ 0.9 V. Figure 2a also shows a similar result with a constant V_{oc} of 1.29 V until about 160 nm, and then it decreases to about 0.9 V when ETL thickness is increased to 200 nm. The fill factor remains unchanged until ETL thickness of 70 nm (Fig. 4c), and beyond that, it decreases to zero as the ETL thickness becomes 200 nm. Similarly, in Fig. 2b, the fill factor remains almost constant up to $\sim$ 70 nm, and reduced to zero as the ETL thickness becomes 200 nm. Also, Figs. 2-b and 4d shows that, until ETL thickness of about 40 nm, cell efficiency remains constant, and beyond that, efficiency becomes zero as the ETL thickness reaches 200 nm due to high series resistance (Fig. 3).

In terms of energy band alignment (Fig. 1) and high V_{oc}, TiO$_2$ suits spiro-OMeTAD well, since it blocks holes from reaching the top electrode, and high V_{oc} is due to the difference between[40] the quasi-Fermi level of electrons in TiO$_2$ and the highest occupied molecular orbital (HOMO) level of spiro-OMeTAD. The effect of ETL doping density is shown in Fig. 5. J_{sc} decreases marginally from 28.72 mA/cm^2 to 28.70 mA/cm^2 (Fig. 5a). This is due to the fact that photogeneration mainly occurs in the MAPbI$_3$ layer, and, hence, J_{sc} is not affected by
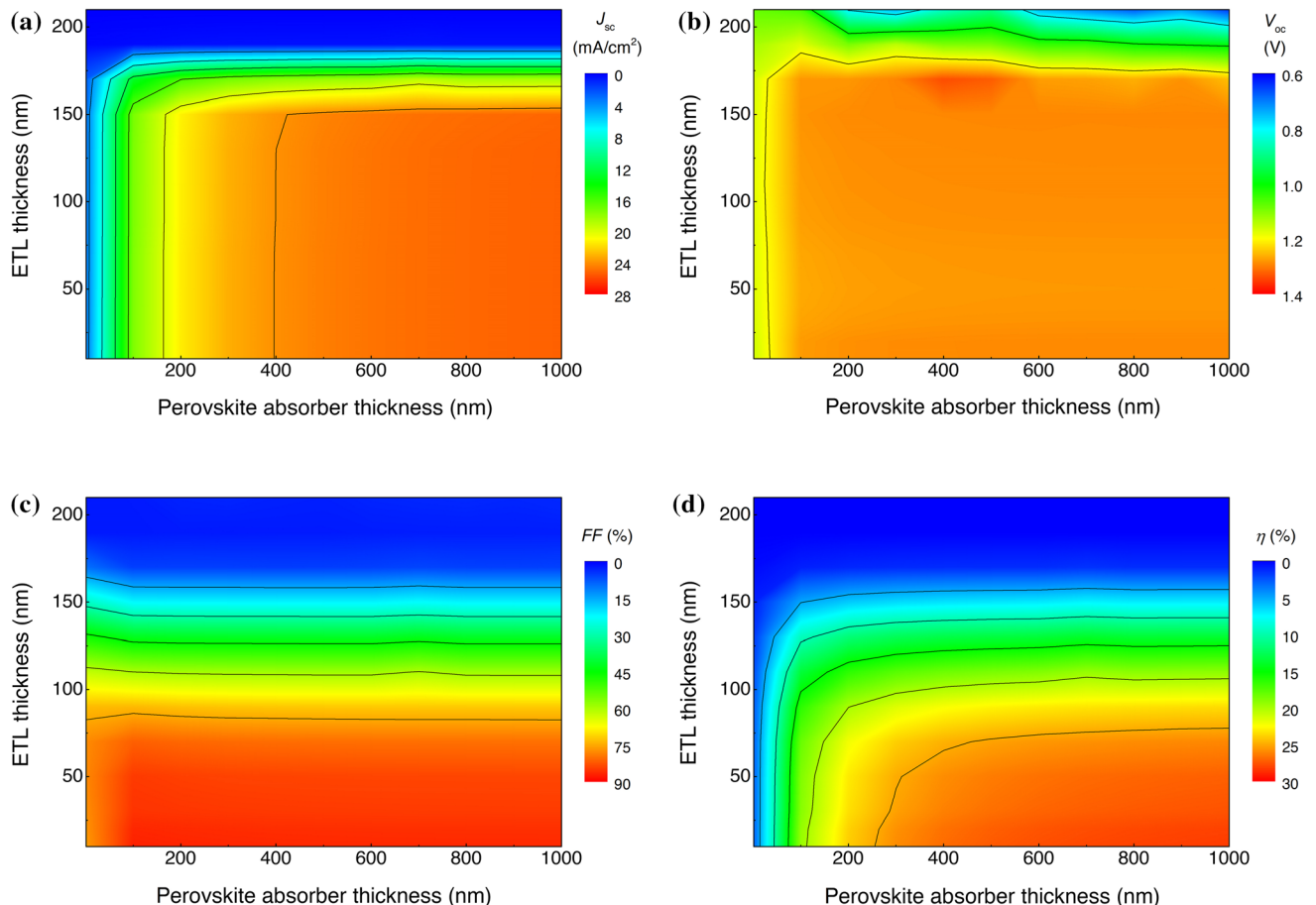

Fig. 4. Contour mapping of (a) J_{sc}, (b) V_{oc}, (c) FF and (d) efficiency. HTL thickness of 200 nm was used in device simulation.
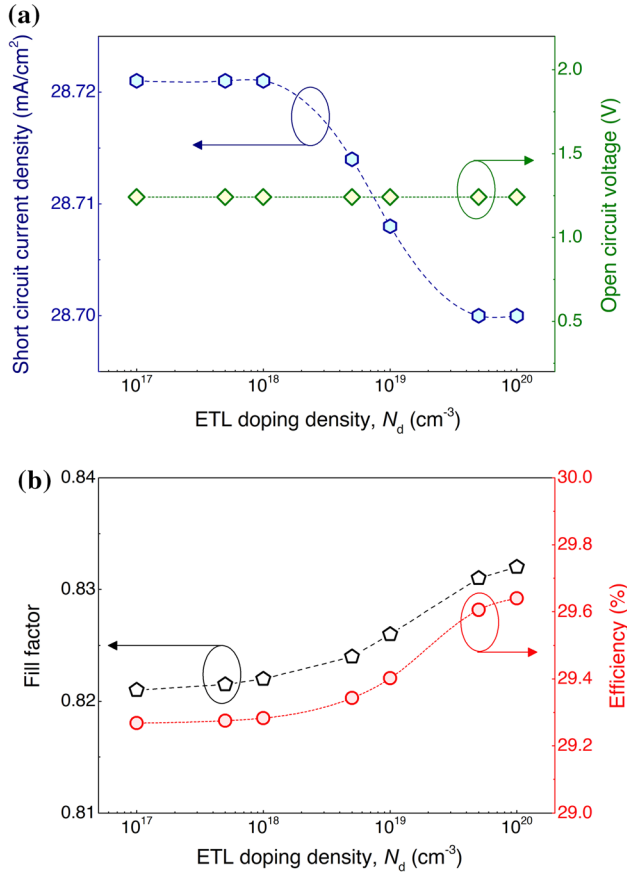
(a)

(b)

Fig. 5. Perovskite solar cell performance: (a) J_{sc} and V_{oc}, (b) fill factor and efficiency as a function of ETL (TiO_2) doping density.
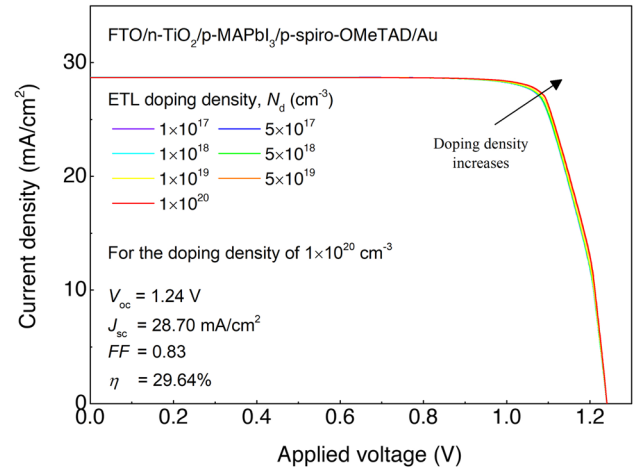

Fig. 6. Light I–V characteristics as a function of ETL doping density. The highest efficiency of 29.64% was achieved for doping density of 10^{20}/cm^3.

ETL doping density. V_{oc} remains constant and independent of doping density, which means that the recombination rate is not affected. This suggests recombination resistance neither increased nor decreased. Figure 5b shows a slight increase in fill factor, and then saturation was observed, which might be due to a reduction in series resistance in the cell. An improvement in efficiency from 29.26% to 29.63% is mainly due to an improvement in the fill factor. Our results suggest that ETL doping density of 10^{20}/cm^3 is suitable for high efficiency, and ohmic losses can be avoided.

Simulated light J–V curves as a function of ETL doping density are shown in Fig. 6. Doping density for the absorber and HTL was fixed as 2.14×10^{17}/cm^3 and 10^{18}/cm^3, respectively. Film thickness of 40 nm, 500 nm and 200 nm was used for the ETL, absorber and HTL, respectively. Figure 6 indicates that J–V characteristics are almost the same, and photovoltaic parameters (J_{sc}, V_{oc}, FF and efficiency) extracted from light J–V curves are almost independent of ETL doping density. For all doping density values between 1×10^{17}/cm^3 and 1×10^{20}/cm^3, with ETL thickness of 40 nm, J_{sc}, V_{oc}, FF and efficiency of 28.70 mA/cm^2, 1.24 V, 0.83 and 29.64% were obtained. The best performance results were observed with ETL thickness of $\leq$ 40 nm. If the ETL

thickness is increased beyond 40 nm, cell efficiency gradually decreases to a minimum due to a decrease in fill factor (Fig. 2b) and an increase in series resistance (Fig. 3).

CONCLUSIONS

The role of ETL thickness and its doping density in cell performance is reported in this work. Cell performance was evaluated by light I–V characteristics. Our results show that high V_{oc} and J_{sc} remain unchanged until ETL thickness of 150–160 nm, which can be attributed to no change in the recombination rate and carrier generation mainly occurring in the perovskite layer. Beyond the thickness of 160 nm, V_{oc} and J_{sc} decreased to 0.88 V and zero, respectively. A similar result was obtained from contour mapping. ETL thickness of $\leq$ 40 nm is required to achieve high J_{sc} and V_{oc}, low series resistance and high fill factor and efficiency. When the thickness is > 40 nm, efficiency decreases gradually due to a decrease in fill factor caused by an increase in series resistance in the cell. Variation in donor concentration from 1×10^{17}/cm^3 to 1×10^{20}/cm^3 has no impact on V_{oc} and J_{sc}; however, it improves the fill factor, which might be due to an improved conductivity and hence an improvement in efficiency. For an optimized device with ETL thickness of 40 nm, ETL donor concentration of 1×10^{20}/cm^3, absorber thickness of 500 nm and HTL thickness of 200 nm, the highest efficiency of 29.64% was obtained with V_{oc}, J_{sc} and fill factor of 1.24 V, 28.70 mA/cm^2 and 0.83, respectively.

In conclusion, the critical parameters are ETL thickness and its doping density. The other critical parameters are absorber (perovskite) thickness, band gap, doping density and HTL thickness and its doping density. Our results show that ETL thickness and doping density around 40 nm and 1×10^{20}/cm^3, respectively, are required. For a perovskite layer, ideal parameters of $\sim$ 500 nm thickness, around 1.4 eV band gap, and acceptor

concentration of 2.14×10^{17}/cm^3 are required. For a p-type spiro-OMeTAD HTL, thickness around 200 nm and doping density of 1×10^{18}/cm^3 are required. This work shows an upper limit for TiO$_2$ (ETL) thickness to be used in a CH$_3$NH$_3$PbI$_3$-based planar perovskite solar cell.

REFERENCES

1. Q. Dong, Y. Fang, Y. Shao, P. Mulligan, J. Qiu, L. Cao, and J. Huang, *Science* 347, 967 (2015).
2. A. Kooijman, L.A. Muscarella, and R.M. Williams, *Appl. Sci.* 9, 1678 (2019).
3. S. Ruhle, *Sol. Energy* 130, 139 (2016).
4. M. Ye, C. He, J. Iocozzia, X. Liu, X. Cui, X. Meng, M. Rager, X. Hong, X. Liu, and Z. Lin, *J. Phys. D Appl. Phys.* 50, 373002 (2017).
5. Y. Zhao, J. Wei, H. Li, Y. Yan, W. Zhou, D. Yu, and Q. Zhao, *Nat. Commun.* (2016). https://doi.org/10.1038/ncomms10228.
6. R.A. Belisle, W.H. Nguyen, A.R. Bowring, P. Calado, X. Li, S.J.C. Irvine, M.D. McGehee, P.R.F. Barnes, and B.C. O'Regan, *Energy Environ. Sci.* 10, 192 (2017).
7. J. Krysa, H. Krysova, Z. Hubicka, S. Kment, J. Maixner, and L. Kavan, *Photochem. Photobiol. Sci.* 18, 891 (2019).
8. H. Hu, B. Dong, H. Hu, F. Chen, M. Kong, Q. Zhang, T. Luo, L. Zhao, Z. Guo, J. Li, Z. Xu, S. Wang, D. Eder, and L. Wan, *ACS Appl. Mater. Interfaces* 8, 17999 (2016).
9. M.M. Lee, J. Teuscher, T. Miyasaka, T.N. Murakami, and H.J. Snaith, *Science* 338, 643 (2014).
10. J. Burschka, N. Pellet, S.J. Moon, R. Humphry-Baker, P. Gao, M.K. Nazeeruddin, and M. Gratzel, *Nature* 499, 316 (2013).
11. M. Seetharaman, P. Nagarjuna, P. Naresh Kumar, S.P. Singh, M. Deepa, and M.A.G. Namboothiry, *Phys. Chem. Chem. Phys.* 16, 24691 (2014).
12. H. Zhu, A.K. Kalkan, J. Hou, and S.J. Fonash, *AIP Conf. Proc.* 462, 309 (1999).
13. Y. Liu, Y. Sun, and A. Rockett, *Sol. Energy Mater. Sol. Cells* 98, 124 (2012).
14. K.L. Kearney and A.A. Rockett, *J. Electrochem. Soc.* 163, H598 (2016).
15. S.J. Fonash, J. Arch, J. Cuiffi, J. Hou, W. Howland, P.J. McElheny, A. Moquin, M. Rogosky, T. Tran, H. Zhu, and F. Rubinelli, *A Manual for AMPS-1D for Windows 95/NT* (Happy Valley: The Pennsylvania State University, 1997).
16. G.A.M. Hurkx, D.B.M. Klaassen, and M.P.G. Knuvers, *IEEE Trans. Electron Devices* 39, 331 (1992).
17. K. Yang, *Solid-State Electron.* 36, 321 (1993).
18. S. Yasar, S. Kahraman, S. Cetinkaya, S. Apaydın, I. Bilican, and I. Uluer, *Optik* 127, 8827 (2016).
19. R. Jeyakumar, A. Bag, and R. Reza Nekovei, *Solar Energy* 190, 104 (2019).
20. W.J. Yin, T.T. Shi, and Y.F. Yan, *Adv. Mater.* 26, 4653 (2014).
21. A. Bag, R. Radhakrishnan, R. Nekovei, and R. Jeyakumar, *Solar Energy* 196, 177 (2020).
22. J. Cui, T. Allen, Y. Wan, J. McKeon, C. Samundsett, D. Yan, X. Zhang, Y. Cui, Y. Chen, P. Verlinden, and A. Cuevasa, *Sol. Energy Mater. Sol. Cells* 158, 115 (2016).
23. P. Löper, M. Stuckelberger, B. Niesen, J. Werner, M. Filipic, S. Moon, J. Yum, M. Topic, S. De Wolf, and C. Ballif, *J. Phys. Chem. Lett.* 6, 66 (2015).
24. M. Filipic, P. Löper, B. Niesen, S. De Wolf, J. Krc, C. Ballif, and M. Topic, *Opt. Express* 23, A263 (2015).
25. G. Xosrovashvilia and N.E. Gorjib, *J. Mod. Opt.* 60, 936 (2013).
26. Q. Zhou, D. Jiao, K. Fu, X. Wu, Y. Chen, J. Lu, and S. Yang, *Sol. Energy* 123, 51 (2016).
27. T. Minemoto and M. Murata, *J. Appl. Phys.* 116, 054505 (2014).
28. A. Poglitsch and D. Weber, *J. Chem. Phys.* 87, 6373 (1987).
29. D. Poplavskyy and J. Nelson, *J. Appl. Phys.* 93, 341 (2003).
30. H.S. Kim, C.R. Lee, J.H. Im, K.B. Lee, T. Moehl, A. Marchioro, S.J. Moon, R.H. Baker, J.H. Yum, J.E. Moser, M. Grätzel, and N.G. Park, *Sci. Rep.* 2, 591 (2012).
31. T. Leijtens, I. Ding, T. Giovenzana, J.T. Bloking, M.D. McGehee, and A. Sellinger, *ACS Nano* 6, 1455 (2012).
32. H.J. Du, W.C. Wang, and J.Z. Zhu, *Chin. Phys. B* 25, 108802 (2016).
33. L. Huang, X. Sun, C. Li, R. Xu, J. Xu, Y. Du, Y. Wu, J. Ni, H. Cai, J. Li, Z. Hu, and J. Zhang, *Sol. Energy Mater. Sol. Cells* 157, 1038 (2016).
34. T. Minemoto and M. Murata, *Sol. Energy Mater. Sol. Cells* 133, 8 (2015).
35. W.A. Laban and L. Etgar, *Energy Environ. Sci.* 6, 3249 (2013).
36. M.I. Hossain, F.H. Alharbi, and N. Tabet, *Sol. Energy* 120, 370 (2015).
37. S.D. Stranks, G.E. Eperon, G. Grancini, C. Menelaou, M.J. Alcocer, T. Leijtens, L.M. Herz, A. Petrozza, and H.J. Snaith, *Science* 342, 341 (2013).
38. L.S. Mende and M. Gratzel, *Thin Solid Films* 500, 296 (2006).
39. A.N. Cho and N.G. Park, *ChemSusChem* 10, 3687 (2017).
40. S.S. Reddy, K. Gunasekar, J.H. Heo, S.H. Im, C.S. Kim, D.H. Kim, J.H. Moon, J.Y. Lee, M. Song, and S.H. Jin, *Adv. Mater.* 28, 686 (2016).